Zhihan Hong

Paper title:

An Integrated Manufacturing System for the Design, Fabrication, and Measurement of Ultra-Precision Freeform Optics

L. B. Kong, C. F. Cheung, W. B. Lee, and S. To

1. Introduction

For the demand of the freeform optics ultra-precision fabrication, the experience and the skills are both important. Through an expensive trial and error approach when new materials, new surface design, or new machine tools are used. In addition, the cutting strategy in ultra-precision machining is extremely important.

In order to make the machining process more predictable and controllable, an alternative approach is to build simulation models to predict and optimize the machining process.

An integrated platform will provide an important means for the optimization of the cutting strategy as well as the prediction of surface generation in ultra-precision machining.

A series of preliminary experiments have been conducted to evaluate the performance of the platform. One application of F-theta lens, which is commonly used in laser scanners and printers, is demonstrated for its optics design, fabrication and measurement by the system. The results show that the proposed integrated platform not only helps to shorten the cycle time for the development of freeform components but also provides an important means for the optimization of the surface quality in the ultra-precision machining of ultra-precision freeform surfaces.

2. Layout of the integrated system

The platform mainly consists of four key modules, which are, as shown in Fig. 1, the optics design module (ODM), the data exchange module (DEM), the machining process simulation and optimization module (MPSOM) and the freeform measurement and evaluation module (FMEM).

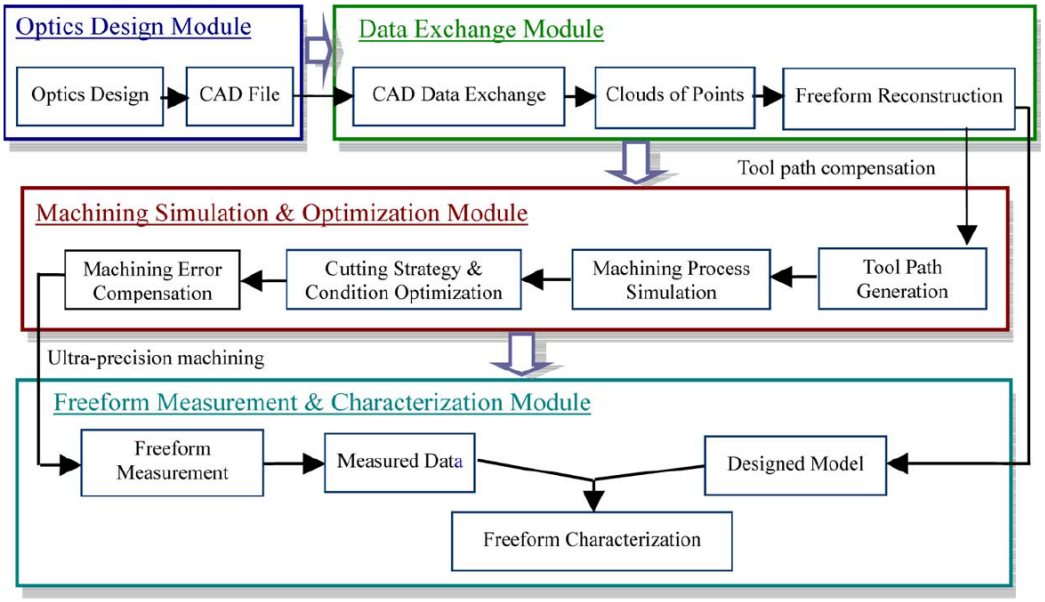

Fig. 1. Layout of the integrated system for freeform optics design, fabrication, and measurement.

As shown in Fig. 1, an optics design module is employed for optics design and simulation of optical performance, and the optics design data can be output as a CAD file for further processing. A precise computation algorithm for freeform control knot vectors has been proposed based on the principle of conservation for edge-ray Etendue [20], as shown in Fig. 2, which can accomplish the design of freeform optics part with optimum efficiency and accuracy light distribution just within a short time period (e.g., a few hours or even shorter).

In Fig. 2, the conservation for edge-ray Etendue can be expressed as

$$E[M(\Sigma_O)] = E[M(\Sigma_I)] = n^2 \int\int dA cos\theta d\Omega$$

where E[.] is the Etendue operation, M(.) means the edge light is the output light, Σ_O is the input light, Σ_I is the refraction index, n is the area of light source, A Ω is the aperture angle, and is the solid angle.

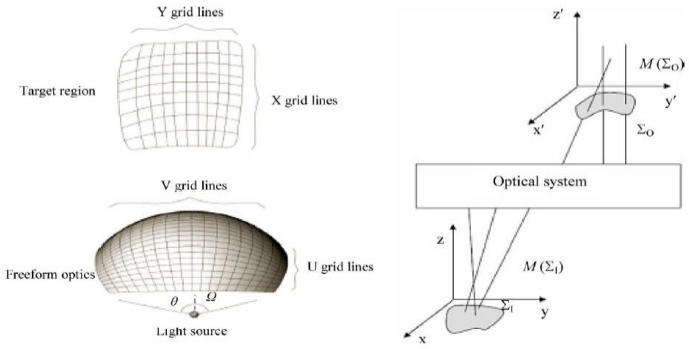

Fig. 2. Conservation for edge-ray Etendue.

Data Exchange Module

The aim of surface reconstruction is to find a continuous surface fitted from the scattered points based on a certain criterion, especially the scattered points from the optics design module, which is used as the designed reference surface for the subsequent freeform machining and characterization.

Fig. 3. Flow chart of freeform reconstruction and optimization module.

Fig. 3 shows the flow chart of freeform reconstruction and optimization. The freeform continuous model is optimized by selecting proper parameters (e.g., the order of polynomial, order and weight of Nurbs, etc.).

Machining Simulation and Optimization Module

Basically, optical freeform surface can be classified as continuous freeform surface and structural freeform surface. A modelbased simulation system has been established to simulate the machining process, predict the surface generation, and optimize

The cutting strategies for the continuous freeform surface and structural freeform surface, the high precision surface quality depends largely on the proper selection of cutting condition parameters and cutting strategies, for example, selecting horizontal cutting or vertical cutting as the cutting strategy, as shown in Fig. 4(a), selecting uni-direction or bi-direction cutting, with or without retreat, as the cutting path planning, as shown in Fig. 4(b).

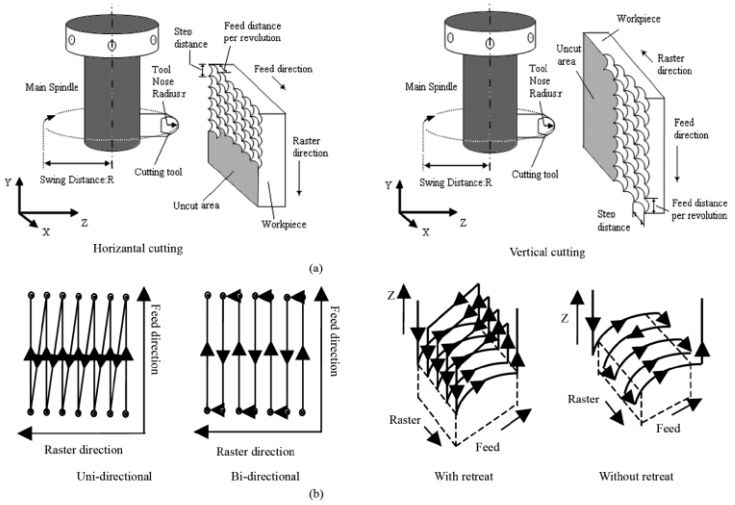

Fig. 4. Machining strategies for ultra-precision raster milling. (a) Cutting Strategies. (b) Cutting path planning.

The surface roughness profile of the machined surface is formed by the repetition of the tool tip making a cut at intervals according to the tool feed rate and then moving a

specified distance by steps under ideal cutting conditions. The feed direction is perpendicular to the raster direction, and both of the directions used in horizontal cutting are opposite to those used in vertical cutting. The generalized equation for the determination of theoretical arithmetic roughness for the different cutting strategies in ultra-precision raster milling is shown as

$$R_a = \frac{c^2}{24R_1} + \frac{\varepsilon^2}{24R_2}$$

Where R1=R and R2=r for horizontal cutting while R1=r and R2=R for vertical cutting; R is the swing distance and r is the tool nose radius.

1) Tool Path Generation Based on the Workpiece Design Surface for Raster Milling: One important step for machining process simulation is the tool path generation, which is also applicable for the real NC program generation. As shown in Fig. 5, cutting point $P_c = (x_c, y_c, z_c)$, tool nose center $P_o = (x_o, y_o, z_o)$, swing center (cutter location, CL) $P_T = (x_T, y_T, z_T)$, surface normalized normal vector at $n_t = (n_x, n_y, n_z)$ cutting point . The swing distance is R and the tool nose radius is . After tool nose radius compensation, the location of tool nose center

$$P_o = P_c + r * (\cos\phi\sin\theta, \sin\phi, \cos\phi\cos\theta) = P_c + r * (n_x, n_y, n_z)$$

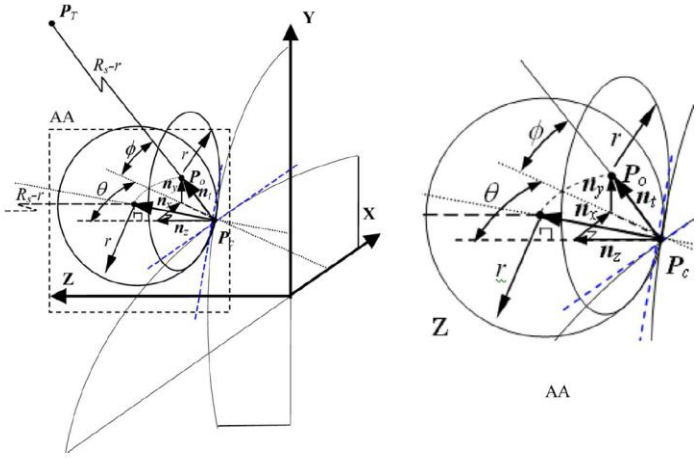

Fig. 5. Compensation of tool nose radius and swing distance for tool path generation in raster milling.

Where ϕ is the angle between the normal vector n_t and the X-Z plane; θ is the angle between the projection of n_t on the X-Z plane and the Z axis. Swing center P_T after the compensation of swing distance

$$P_T = P_o + (R - r) * (\sin\theta, 0, \cos\theta) = P_o + (R - r) * \left(\frac{n_x}{\sqrt{n_x^2 + n_x^2}}, 0, \frac{n_z}{\sqrt{n_x^2 + n_x^2}}\right)$$

$$= \begin{cases} x_c + r * n_x + (R - r) * \dfrac{n_x}{\sqrt{n_x^2 + n_x^2}} \\ y_c + r * n_y \\ z_c + r * n_z + (R - r) * \dfrac{n_z}{\sqrt{n_x^2 + n_x^2}} \end{cases}$$

And based on the flow diagram:

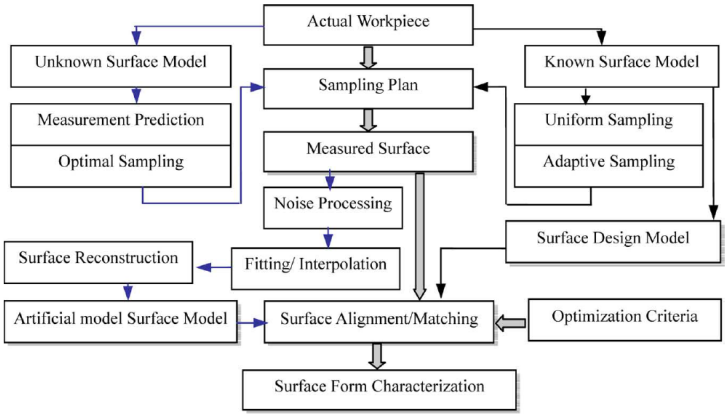

Fig. 6. Flow chart of integrated freeform characterization method.

EXPERIMENTAL AND IMPLEMENTATION RESULTS

One experiment has been conducted to study the surface roughness by raster milling, to further validate the roughness model in the proposed platform. Fig. 9 shows the design of the workpiece used in the cutting test. Fig. 9(a) shows the dimension of the workpiece, and (b) is the produced workpiece. As shown in Fig. 9(b).

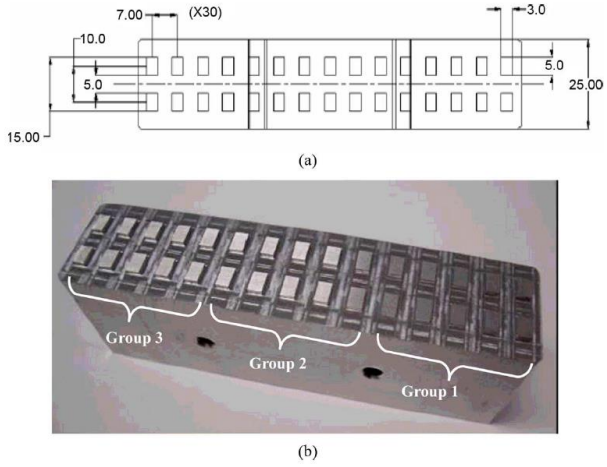

Fig. 9. Workpiece for studying the effect of machining parameters. (a) Dimension of the workpiece design (unit: mm). (b) Machined workpiece.

Wyko NT8000 optical measurement system. Fig. 10 shows predicted and measured surface roughness (Ra). It is interesting to note that the predicted values show a good agreement or similar trend with the measured results. There exist some deviations between the measured values and the predicted ones, especially in the studies of spindle speed and feed rate as shown in Fig. 10(a) and (b). This can be explained as that the surface generation in raster milling process is also affected by other factors such as relative vibration between cutting tool and workpiece, material swelling, etc. Besides, with the increasing of spindle speed, much more vibration is caused, which limits the

improvement of the surface quality. The experimental results are helpful for the optimization of machining parameters to obtain good surface quality and high machining efficiency at the same time, by finding out the optimum cutting conditions.

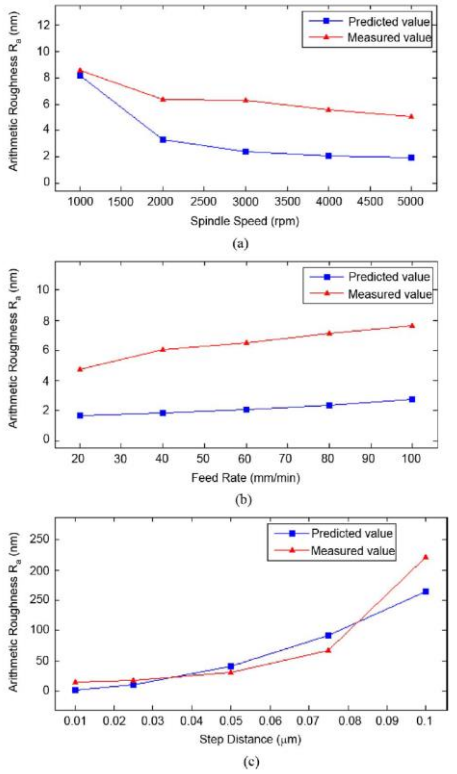

Fig. 10. Predicted and measured surface roughness by raster milling. (a) Spindle speed versus surface roughness (Ra). (b) Feed rate versus surface roughness (Ra). (c) Step distance versus surface roughness (Ra).

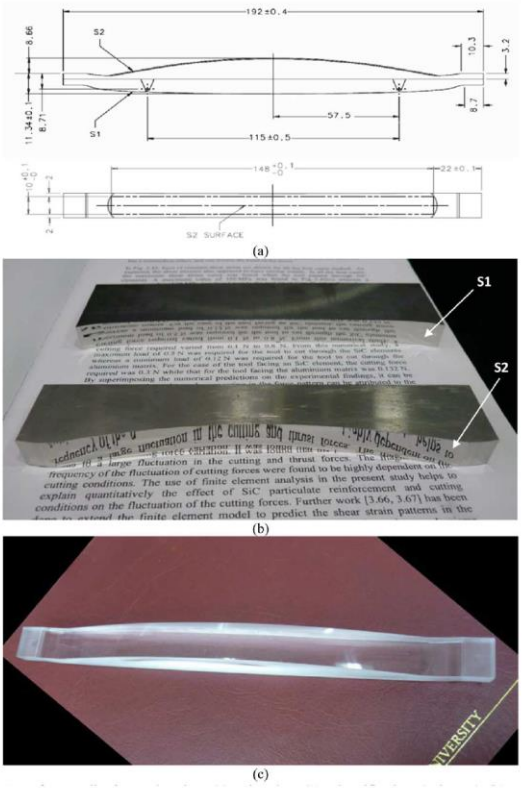

Fig. 11. Freeform application: F-theta lens. (a) F-theta lens CAD Specifications (unit: mm). (b) F-theta mould insert. (c) F-theta mould injection product.

The F-theta lens, which is commonly applied to laser scanners or copiers, is a typical example of optical freeform surface. The surface representation of the F-theta lens can be defined by an anamorphic aspheric surface. For the two side surfaces (S1, S2) of the F-theta Lens, the parameters are defined in Table II. The F-theta surface workpiece was fabricated using the multi-axis freeform machining system mentioned in the previous section. The machining parameters are shown in Table III. Fig. 11 shows the freeform application: F-theta lens.

3. Conclusion

In this paper, the technological development of an integrated system for optical design, ultra-precision machining, and precision measurement of freeform optical surfaces is presented. With the successful development of the platform, the optimal machining parameters and strategies can be obtained. The machining and measuring process can be simulated on the computer and the verified data can then be input into the advanced CNC ultra-precision machine for machining the components. This results in shortening the cycle time for product development and in improving the quality of the product without the need for time-consuming and expensive trial-and-error cutting tests.

4. Reference

[1] Harnessing Light: Optical Science and Engineering for the 21st Century. Washington, DC: National Research Council (ed.) National Academic Press, 1998.
[2] K. I. Kim and K. Kim, “A new machine strategy for sculptured surfaces using offset surface,” Int. J. Prod. Res., vol. 33, no. 6, pp. 1683–1697,
1995.
[3] A. M. Ramos, C. Relvas, and J. A. Simões, “The influence of finishing milling strategies on texture, roughness and dimensional deviations on the machining of complex surfaces,” J. Mater. Process. Technol., vol. 136, pp. 209–216, 2003.
[4] Y. W. Sun, D. M. Guo, and Z. Y. Jia, “Spiral cutting operation strategy for machining of sculptured surfaces by conformal map approach,” J. Mater. Process. Technol., vol. 180, pp. 74–82, 2006.
[5] H. El-Mounayri, M. A. Elbestawi, A. D. Spence, and S. Bedi, “General geometric modelling approach for machining process simulation,” Int. J. Adv. Manuf. Technol., vol. 13, pp. 237–247, 1997.
[6] T. Bailey, M. A. Elbestawi, T. I. El-Wardany, and P. Fitzpatrick, “Generic simulation approach for multi-axis machining, part 1: Modeling
methodology,” J. Manuf. Sci. Eng., vol. 124, no. 3, pp. 624–633, 2002.
[7] T. Bailey, M. A. Elbestawi, T. I. El-Wardany, and P. Fitzpatrick, “Generic simulation approach for multi-axis machining, part 2: Model
calibration and feed rate scheduling,” J. Manuf. Sci. Eng., vol. 124, no. 3, pp. 634–642, 2002.
[8] Y. Lin and Y. Shen, “Modelling of five-axis machine tool metrology models using the matrix summation approach,” Int. J. Adv. Manuf. Technol., vol. 21, pp. 243–248, 2003.
[9] K. Weinert, S. J. Du, P. Damm, and M. Stautner, “Swept volume generation for the simulation of machining processes,” Int. J. Mach. Tools Manuf., vol. 44, no. 6, pp. 617–628, 2004.
[10] C. Lartigue, E. Duc, and C. Tournier, “Machining of free-form surfaces and geometrical specifications,” Proc. Inst. Mech. Eng., vol. 213, pt.
Part B, pp. 21–27, 1998.
[11] E. Duc, C. Lartigue, C. Tournier, and P. Bourdet, “A new concept for the design and the manufacturing of free-form surfaces: The machining surface,”CIRP Ann. -Manuf. Technol., vol. 48, no. 1, pp. 103–106, 1999.
[12] R. Zhu, S. G. Kapoor, and R. E. DeVor, “Mechanistic modeling of the ball end milling process for multi-axis machining of free-form surfaces,” J. Manuf. Sci. Eng., vol. 123, no. 3, pp. 369–379, 2001.
[13] C. Brecher, S. Lange, M. Merz, F. Niehaus, C. Wenzel, M. Winterschladen, and M. Weck, “NURBS based ultra-precision free-form machining,” CIRP Ann.-Manuf. Technol., vol. 55, no. 1, pp. 547–550, 2006.
[14] G. Elbert and E. Cohen, “Tool path generation for freeform surface models,” in 2nd ACM Solid Modeling 93-5/93, Montreal, Canada,
1993, pp. 419–428.
[15] L. Zhang, J. Deng, and S. C.-F. Chan, “A next generation NC machining system based on NC feature unit and real-time tool-path generation,”
Int. J. Adv. Manuf. Technol, vol. 16, pp. 889–901, 2000.
[16] W. B. Lee, S. To, and C. F. Cheung, Design and Advanced Manufacturing Technology for Freeform Optics. Hong Kong: Hong Kong
Polytechnic Univ., 2005, p. 237.
[17] W. B. Lee, C. F. Cheung, S. To, D. Gao, and S. J. Wang, “An investigation of fast tool servo machining of optical microstructures,” Nanotechnol. Prec. Eng., vol. 3, no. 3, pp. 216–221, 2005.
[18] C. F. Cheung, W. B. Lee, B. Wang, and J. B. Jiang, Design and Fabrication of Electronic and Optical Systems for Advanced Automotive
Lighting. Hong Kong: The Hong Kong Polytechnic University, 2007, vol. 2, Advanced Optics, p. 282.
[19] J. B. Jiang, S. To, W. B. Lee, and B. Cheung, “Design of the freeform V-cut optics in the cell phone backlight system,” Chinese J. Liquid
Crystals Displays, vol. 20, no. 3, pp. 178–184, 2005.
[20] J. B. Jiang, C. F. Cheung, S. To, K. W. Cheng, H. Wang, and W. B. Lee, “Design and fabrication of freeform reflector for automotive headlamp,” in Proc. 2nd Int. Conf. Power Electron. Syst. Applicat., Hong Kong, Nov. 12–14,2006, , pp. 220–224.